ORIGINAL PAPER

Power harvesting from transverse galloping of square cylinder

**Abdessattar Abdelkefi · Muhammad R. Hajj ·
Ali H. Nayfeh**

Abstract The concept of exploiting galloping of square cylinders to harvest energy is investigated. The energy is harvested by attaching a piezoelectric transducer to the transverse degree of freedom. A representative model that accounts for the coupled cylinder displacement and harvested voltage is used to determine the levels of the harvested power. The focus is on the effect of the Reynolds number on the aerodynamic force, the onset of galloping, and the level of the harvested power. The quasi steady approximation is used to model the aerodynamic loads. A linear analysis is performed to determine the effects of the electrical load resistance and the Reynolds number on the onset of galloping, which is due to a Hopf bifurcation. We derive the normal form of the dynamic system near the onset of galloping to characterize the type of the instability and to determine the effects of the system parameters on its outputs near the bifurcation. The results show that the electrical load resistance and the Reynolds number play an important role in determining the level of the harvested power and the onset of galloping. The results also show that the maximum levels of harvested power are accompanied with minimum transverse displacements for both low- and high-Reynolds number configurations.

A. Abdelkefi · M.R. Hajj (✉) · A.H. Nayfeh
Virginia Tech, Blacksburg, VA, USA
e-mail: mhajj@vt.edu

1 Introduction

Converting ambient and aeroelastic vibrations, using piezoelectric transducers, to electric power has been proposed for powering micro-electromechanical systems [1, 2] and heath monitoring and wireless sensors [3] and for replacing small batteries that have a finite life span and require hard and expensive maintenance [4, 5]. To date, most of energy harvesting from mechanical vibrations concentrated on exploiting ambient vibrations [6–12]. More recently, few investigations [13–20] focused on the conversion of aeroelastic vibrations of wings to electrical power. These investigations have been mostly concerned with aeroelastic responses of streamlined surfaces, such as wings. In comparison to wing flutter, the galloping aeroelastic instability results in large oscillations. This is very beneficial when using piezoelectric transducers because the harvested voltage is directly related to the oscillation amplitude.

As the wind speed exceeds a critical value, an elastic bluff body undergoes transverse oscillations, called galloping. Den Hartog [21] was the first to study and explain the galloping phenomenon. He used the quasi steady hypothesis to describe the aerodynamic

loads. He also developed a criterion for the occurrence of galloping. Several studies [22–33] investigated the effects of various parameters on the behavior of the galloping of different structures. Barrero-Gil et al. [34] investigated theoretically the possibility of using transverse galloping to extract energy. Specific methods on how to harvest this energy were not discussed. Based on previous numerical and experimental data, Barrero-Gil et al. [33, 34] modeled the transverse aerodynamic force using a cubic polynomial for high Reynolds numbers and a seven-order polynomial for Reynolds numbers below 200. Barrero-Gil et al. [33] investigated the possibility of transverse galloping of a square cylinder at low Reynolds numbers ($Re < 200$). They showed that a square cylinder cannot gallop below a Reynolds number of 159.

The objective of this work is to investigate the possibility of designing enhanced piezoelectric energy harvesters that exploit the galloping of square cylinders. Particularly, we aim to determine the power levels that can be generated from these oscillations for low and high Reynolds numbers by modeling the aerodynamic loads using the quasi steady approximation. To this end, we attach a piezoelectric transducer to the transverse degree of freedom of the cylinder. We develop a phenomenological model for the global coupled (transverse displacement and electrical circuit) system in Sect. 2. In Sect. 3, we perform a linear analysis to determine the effects of the electrical load resistance and the Reynolds number on the onset of galloping, which is due to a Hopf bifurcation. In Sect. 4, we perform a nonlinear analysis, based on the normal form of this bifurcation, to determine the effects of the load resistance and the Reynolds number on the harvested power, voltage output, and transverse displacement. Conclusions are presented in Sect. 5.

2 Mathematical modeling of transverse galloping

We consider a galloping-based piezo-aeroelastic energy harvester consisting of an elastically-mounted square cylinder and a piezoelectric transducer attached to its transverse degree of freedom, as shown in Figs. 1(a) and 1(b). When this system is subjected to an incoming flow, the cylinder undergoes galloping in the transverse direction as the wind speed exceeds a critical value. The governing equations of the coupled electromechanical system are written as

$$m\left(\ddot{y} + 2\xi\omega_n\dot{y} + \omega_n^2 y\right) - \theta V = F_y = \frac{1}{2}\rho U^2 D C_y \quad (1)$$

$$C_p\dot{V} + \frac{V}{R} + \chi\dot{y} = 0 \tag{2}$$

where m is the total mass per unit length, D is the characteristic dimension of the body normal to the incoming flow, U is the velocity of the incoming flow, ρ is the fluid density, ω_n is the cylinder natural frequency, ξ is the mechanical damping ratio, θ and χ are the electromechanical coupling coefficients, V is the harvested voltage across the load resistance R, C_p is the capacitance of the piezoelectric layer, and F_y and C_y are respectively the aerodynamic force per unit length and force coefficient in the normal direction to the incoming flow.

Generally, in transverse galloping, the characteristic time scale of the structure oscillation, which is approximately equal to $\frac{2\pi}{\omega_n}$, is much larger than the characteristic time scale of the flow which is O($\frac{D}{U}$). Furthermore, if the vortex shedding frequency is much larger than the natural frequency of the oscillating square cylinder, the quasi steady hypothesis can be used to evaluate the aerodynamic force [26]. In this work, we consider two configurations that cover low and high Reynolds number (Re) regimes of galloping square cylinders. For Reynolds numbers below 200, Barrero-Gil et al. [33] showed that the transverse aerodynamic force can be estimated by the odd terms in a seven-order polynomial function of $\frac{\dot{y}}{U}$, that is,

$$F_y = \frac{1}{2}\rho U^2 D\left[a_1\frac{\dot{y}}{U} + a_3\left(\frac{\dot{y}}{U}\right)^3\right.$$
$$\left. + a_5\left(\frac{\dot{y}}{U}\right)^5 + a_7\left(\frac{\dot{y}}{U}\right)^7\right] \tag{3}$$

Here, $\frac{\dot{y}}{U} = \tan\alpha$, where α is the angle of attack. Based on the numerical results of Sohankar et al. [35], the coefficients in Eq. (3) are estimated by Barrero-Gil et al. [33] as
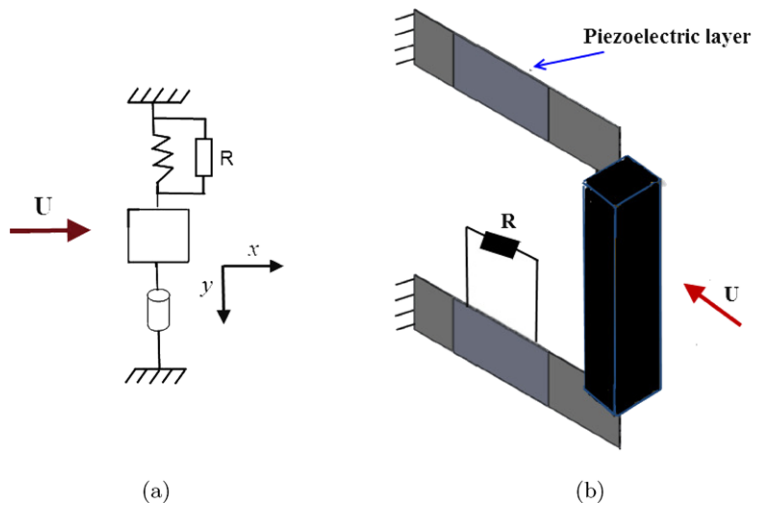
$$a_1 = -2.7 + 0.017Re,$$

$$a_3 = 10 - 0.096Re - 0.001Re^2,$$

$$a_5 = -24 - 0.21Re + 0.011Re^2,$$

$$a_7 = 13 + 1.1Re - 0.024Re^2$$

Fig. 1 (**a**) Simplified and (**b**) three-dimensional schematics of piezo-aeroelastic energy harvester based on transverse galloping of a square cylinder

The aerodynamic coefficient C_y is directly related to the lift and drag coefficients C_l and C_d, respectively, by $C_y = -[C_l \cos(\alpha) + C_d \sin(\alpha)]$.

At high Reynolds numbers, Barrero-Gil et al. [34] showed that the aerodynamic force coefficient can be approximated by a cubic polynomial expansion of $\frac{\dot{y}}{U}$ with the coefficients being independent of the Reynolds number. Then the transverse aerodynamic force can be written in the form

$$F_y = \frac{1}{2}\rho U^2 D \left[a_1 \frac{\dot{y}}{U} + a_3 \left(\frac{\dot{y}}{U} \right)^3 \right] \quad (4)$$

where a_1 and a_3 are empirical coefficients obtained by fitting C_y with a cubic polynomial of $\dot{y}/U$.

The Den Hartog stability criterion [21] states that a section of a structure on a flexible support is susceptible to galloping when the linear coefficient a_1 is positive. For the energy harvester considered here, the onset of galloping is determined when the electromechanical damping of the system changes from a positive to a negative value. The nonlinear coefficient a_3 is always negative, because as the angle of attack increases, C_y increases, achieves a maximum value, and then decreases. For this work, our focus is on a square cylinder. The linear and nonlinear coefficients used to determine the transverse aerodynamic force are empirically determined from the experiments of Parkinson and Smith [22]; that is, $a_1 = 2.3$ and $a_3 = -18$.

Two different configurations are considered in this work: low and high Reynolds number configurations. In the low Reynolds number configuration, D is set equal to 1 mm, $m = 0.044$ kg, $\omega_n = 10$ rad/s, $\xi =$

7.102×10^{-6}, and the speed is limited to a maximum value of 2 m/s so that the Reynolds number remains below 200. The galloping parameters in this configuration are the same as those used by Barrero-Gil et al. [33]. The transverse aerodynamic force is estimated by Eq. (3). In the high Reynolds number configuration, D is set equal to 1.5 cm, $m = 0.44$ kg, $\omega_n = 62.83$ rad/s, and $\xi = 0.0013$.

3 Effects of the electrical load resistance and Reynolds number on the onset of galloping

Introducing the piezoelectric transducer and load resistance causes the global frequency and damping of the electromechanical system to be different from those of the mechanical system (without the piezoelectric transducer). These effects can be determined from the analysis of the linear system in which only the first term of the aerodynamic force is considered. Introducing the following state variables:

$$\mathbf{X} = \begin{bmatrix} X_1 \\ X_2 \\ X_3 \end{bmatrix} = \begin{bmatrix} y \\ \dot{y} \\ V \end{bmatrix} \quad (5)$$

we rewrite the linear part of the coupled equations of motion as

$$\dot{X}_1 = X_2 \quad (6)$$

$$\dot{X}_2 = -\left(2\xi\omega_n - \frac{\rho U D a_1}{2m} \right) X_2 - \omega_n^2 X_1 + \frac{\theta}{m} X_3 \quad (7)$$

$$\dot{X}_3 = -\frac{1}{RC_p}X_3 - \frac{\theta}{C_p}X_2 \tag{8}$$

Clearly, these equations have the form

$$\dot{\mathbf{X}} = B\mathbf{X} \tag{9}$$

where

$$B = \begin{bmatrix} 0 & 1 & 0 \\ -\omega_n^2 & -(2\xi\omega_n - \frac{1}{2}\frac{\rho U D a_1}{m}) & \frac{\theta}{m} \\ 0 & -\frac{\theta}{C_p} & -\frac{1}{RC_p} \end{bmatrix}$$

and $a_1 = -2.7 + 0.017Re$ in the low Reynolds number configuration and $a_1 = 2.3$ in the high Reynolds number configuration.

The matrix $B(U)$ has a set of three eigenvalues λ_i, $i = 1, 2, 3$. The first two eigenvalues are similar to those of a pure galloping problem in the absence of the piezoelectricity effect. The third eigenvalue is a result of the electromechanical coupling. This eigenvalue (λ_3) is always real negative as in the case of piezoelectric systems subjected to base or aeroelastic excitations [10–12, 17]. The first two eigenvalues are complex conjugates ($\lambda_2 = \overline{\lambda_1}$). The real part of these eigenvalues represents the damping coefficient and the positive imaginary part corresponds to the global frequency of the coupled system. Because λ_3 is always real negative, the stability of the trivial solution depends only on the first two eigenvalues. The trivial solution is asymptotically stable if the real part of λ_1 is negative. On the other hand, if the real part of λ_1 is positive, the trivial solution is unstable. The speed U_g for which $\lambda_1 = 0$ corresponds to the onset of instability or galloping. The matrix B also includes all parameters that affect the linear part of the system. This matrix is used to investigate the effects of the load resistance and the Reynolds number on the onset of galloping.

Figure 2 shows the effect of the electrical load resistance on the onset speed of galloping for both configurations. We note that, in the low Reynolds configuration, the galloping speed increases with the load resistance to about 2 m/s, corresponding to $Re = 200$, at about 300 Ω. In the absence of the piezoelectric transducer, Barrero-Gil et al. [33] showed that the considered square cylinder does not gallop below a Reynolds number of 159. For the short-circuit configuration in which the load resistance is very small (approximately 10 Ω), our predicted Reynolds number for the onset of
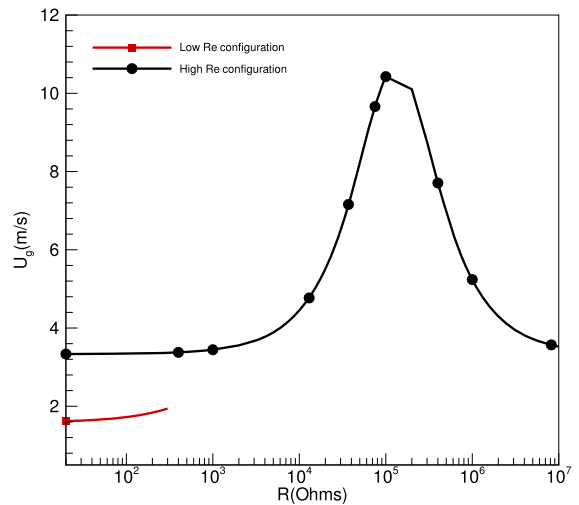

Fig. 2 Variations of the galloping speed with the load resistance for both low and high Reynolds number configurations

galloping matches that obtained by Barrero-Gil et al. [33].

For the high Reynolds numbers, the onset speed of galloping increases as the load resistance increases from low values. It reaches a maximum value near $R = 10^5$ Ω and decreases to lower speeds for load resistances near 10^7 Ω, as shown in Fig. 2. In the absence of the piezoelectric transducer, using the Krylov–Bogoliuvov method, Barrero-Gil et al. [34] showed that the onset speed of galloping depends on the damping ratio ξ, the dimensionless mass ration m^*, and the linear coefficient a_1 by the following relation: $U^* = 4m^*\xi/a_1$ where $U^* = U/(\omega_n D)$ and $m^* = m/(\rho D^2)$. For the short-circuit configuration, our onset speeds of galloping match those obtained by Barrero-Gil et al. [34].

4 Nonlinear analysis

4.1 Effect of higher-order terms in the aerodynamic load

In Fig. 3, we compare the level of the harvested power when modeling the transverse aerodynamic force using all terms in Eq. (3) with those obtained when the higher-order terms a_5 and a_7 are neglected. The results show that, for low wind speeds, the first and third terms are sufficient for predicting the bifurcation and characterizing the system behavior and instability.
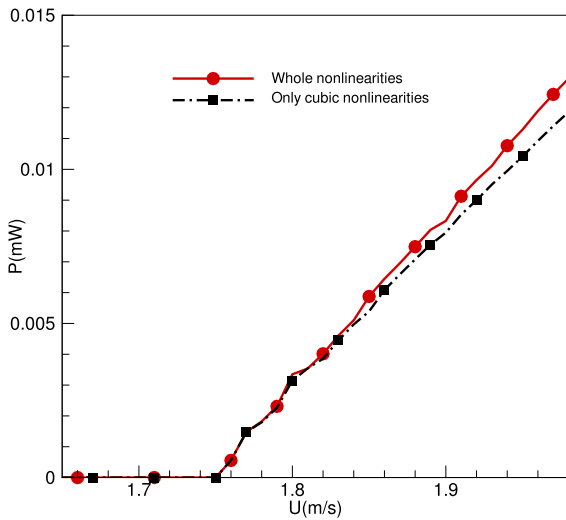
Fig. 3 Effect of the higher-order nonlinear terms in the model of the aerodynamic force, Eq. (3), on the harvested power when $R = 100\,\Omega$

However, for higher wind speeds, between 1.85 m/s and 2 m/s, the level of harvested power is underpredicted when the fifth- and seventh-order terms are neglected. Furthermore, we note that there is no hysteresis when including these higher-order nonlinear terms unlike other systems in which such nonlinear terms resulted in the appearance of hysteresis and unstable branches [36].

4.2 Normal form of Hopf bifurcation

Next, we perform a nonlinear analysis of the coupled system to determine the type of instability or bifurcation associated with the proposed galloping-based harvesters. To this end, we add a perturbation term $\sigma_U U_f$ to the onset speed and express the air speed as $U = U_f + \sigma_U U_f$. Using this expansion, we rewrite the matrix $B(U)$ as

$$B(U) = B(U_f) + \sigma_U B_1(U_f)$$

where

$$B_1(U_f) = \begin{bmatrix} 0 & 0 & 0 \\ 0 & \frac{\rho D(b_1 U_f + 2b_2 U_f^2)}{2m} & 0 \\ 0 & 0 & 0 \end{bmatrix}$$

and b_1 and b_2 are related to the linear coefficient a_1 by $a_1 = b_1 + b_2 U$. For the low Reynolds number configuration, b_1 and b_2 are set equal to -2.7 and 1.7,

respectively; and for the high Reynolds number configuration, b_1 and b_2 are set equal to 2.3 and 0, respectively. Neglecting the higher-order terms (i.e., a_5 and a_7) in the low Reynolds number configuration, we write the equations of motion for both configurations in the following form:

$$\dot{\mathbf{X}} = B(U_f)\mathbf{X} + \sigma_U B_1(U_f)\mathbf{X} + \mathbf{C}(\mathbf{X}, \mathbf{X}, \mathbf{X}) \qquad (10)$$

where

$$\mathbf{C}^T = \left[0, \frac{\rho D(b_3 + b_4 U_f + b_5 U_f^2)}{2m U_f} X_2^3, 0 \right]$$

where b_3, b_4, and b_5 are related to the nonlinear coefficient a_3 by $a_3 = b_3 + b_4 U + b_5 U^2$. For the low Reynolds number configuration, b_3, b_4, and b_5 are set equal to 10, -9.6, and -10, respectively. For the high Reynolds number configuration, b_3, b_4, and b_5 are set equal to -18, 0, and 0, respectively.

Letting G be the matrix whose columns are the eigenvectors of the matrix $B(U_f)$ corresponding to the eigenvalues $\pm j\omega_1$ and $-\mu_3$ and defining a new vector $\mathbf{Y}$ such that $\mathbf{X} = G\mathbf{Y}$, we rewrite Eq. (10) as

$$G\dot{\mathbf{Y}} = B(U_f)G\mathbf{Y} + \sigma_U B_1(U_f)G\mathbf{Y} \\ + \mathbf{C}(G\mathbf{Y}, G\mathbf{Y}, G\mathbf{Y}) \qquad (11)$$

Multiplying Eq. (11) from the left by the inverse G^{-1} of G yields

$$\dot{\mathbf{Y}} = J\mathbf{Y} + \sigma_U K\mathbf{Y} + G^{-1}\mathbf{C}(G\mathbf{Y}, G\mathbf{Y}, G\mathbf{Y}) \qquad (12)$$

where $K = G^{-1}B_1(U_f)G$ and $J = G^{-1}B(U_f)G$ is a diagonal matrix whose elements are the eigenvalues $\pm j\omega_1$ and $-\mu_3$. We note that $Y_2 = \overline{Y_1}$, and hence Eq. (12) can be written in component form as

$$\dot{Y}_1 = j\omega_1 Y_1 + \sigma_U \sum_1^3 K_{1i} Y_i + N_1(\mathbf{Y}) \qquad (13)$$

$$\dot{Y}_3 = -\mu_3 Y_3 + \sigma_U \sum_1^3 K_{3i} Y_i + N_3(\mathbf{Y}) \qquad (14)$$

where the $N_i(\mathbf{Y})$ are trilinear functions of the components of $\mathbf{Y}$.

According to the center-manifold theorem [37], there exists a center manifold

$$Y_3 = H_3(Y_1, \bar{Y}_1)$$

such that the dynamics on this manifold is similar to the dynamics of the system represented by Eqs. (13) and (14). Equation (14) is then rewritten as

$$\dot{Y}_1 = j\omega_1 Y_1 + \sigma_U(K_{11}Y_1 + K_{12}\bar{Y}_1 + K_{13}H_3)$$
$$+ N_1(H_1, \bar{H}_1, Y_3, \bar{Y}_3, H_3) \qquad (15)$$

Because σ_U is small and N_1 and N_3 are cubic functions of the components of $\mathbf{Y}$, H_3 is zero to the third approximation. Keeping only the resonance terms [37] in Eq. (15), we obtain the complex-valued normal form

$$\dot{Y}_1 = j\omega_1 Y_1 + \sigma_U K_{11} Y_1 + \alpha_e Y_1^2 \bar{Y}_1 \qquad (16)$$

where α_e depends on the cubic nonlinear coefficients b_3, b_4, and b_5, as shown in Table 1 for both Reynolds number configurations when the load resistance is set equal to 10^4 Ω.

Next, we express Y_1 in the polar form

$$Y_1 = \frac{1}{2}ae^{j(\omega_1 t + \gamma)} \qquad (17)$$

where a is the amplitude of oscillation and γ is its phase. Substituting Eq. (17) into Eq. (16) and separating the real and imaginary parts, we obtain the following real-valued normal form of the Hopf bifurcation:

$$\dot{a} = \beta_r a + \frac{1}{4}\alpha_{er}a^3 \qquad (18)$$

$$\dot{\gamma} = \beta_i + \frac{1}{4}\alpha_{ei}a^2 \qquad (19)$$

where $\beta = \sigma_U K_{11}$ and the subscripts r and i denote the real and imaginary parts, respectively.

Equation (18) has three equilibrium solutions:

$$a = 0 \quad \text{and} \quad a = \pm\sqrt{\frac{-4\beta_r}{\alpha_{er}}}$$

where $a = 0$ is the trivial solution. The two other solutions are nontrivial. The origin is asymptotically stable for $\beta_r < 0$ or $\beta_r = 0$ and $\alpha_{er} < 0$, unstable for $\beta_r > 0$ or $\beta_r = 0$ and $\alpha_{er} > 0$. The nontrivial solutions exist when $\beta_r\alpha_{er} < 0$. They are stable (supercritical Hopf bifurcation) for $\beta_r > 0$ and $\alpha_{er} < 0$ and unstable (subcritical Hopf bifurcation) for $\beta_r < 0$ and $\alpha_{er} > 0$.

The effective nonlinearity α_e is a function of the system parameters, including the load resistance and the linear and nonlinear coefficients a_1, b_3, b_4, and b_5. Table 1 shows β_r and α_{er} when the electrical load resistance is set equal to 100 Ω for the low Reynolds number configuration and 10^4 Ω for the high Reynolds number configuration.

For the low Reynolds number configuration, we note that the effective nonlinearity depends on b_3, b_4, and b_5. On the other hand, for the high Reynolds number configuration, it depends only on b_3 because the nonlinear coefficient in this configuration is independent of the Reynolds number. For the proposed values of the b_i, we note that the instability is a supercritical Hopf bifurcation for both configurations, as presented in Table 1.

The transverse displacement y, the voltage output V, and harvested power P are related to the amplitude a of the limit cycle by

$$y = a\sqrt{G[1,1]_r^2 + G[1,1]_i^2} \qquad (20)$$

$$V = a\sqrt{G[3,1]_r^2 + G[3,1]_i^2} \qquad (21)$$

$$P = \frac{V^2}{R} \qquad (22)$$

where $(\cdot)_r$ and $(\cdot)_i$ denote the real part and imaginary part, respectively. To validate this analytical solution (normal form of Hopf bifurcation), we compare in Fig. 4 its predictions with those obtained by numerically integrating the high Reynolds number configuration when the electrical load resistance is set equal to $R = 10^4$ Ω. The results show that the normal form
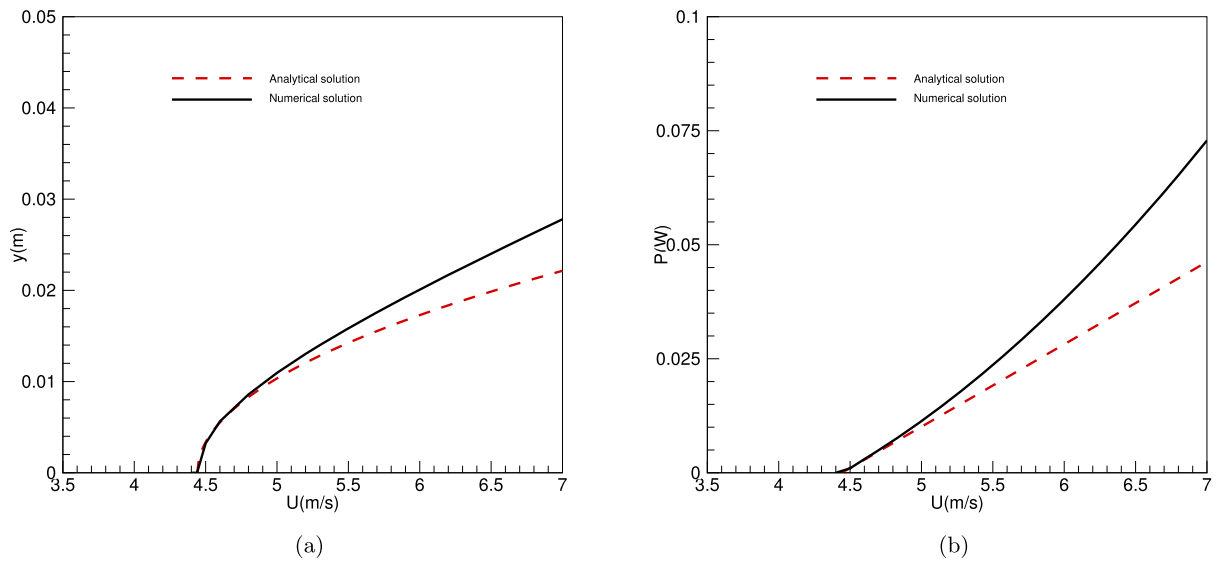
Table 1 Values of the onset speed of galloping and the real parts of β and α_e when $R = 100$ Ω and $R = 10^4$ Ω for the low and high Reynolds number configurations, respectively

Parameters	Low Reynolds number configuration	High Reynolds number configuration
U_f (m/s)	1.723	4.441
β_r	0.03864	0.1088
α_{er}	0.01196 b_3 + 0.02061 b_4 + 0.0355 b_5	0.0000299 b_3
α_{er}	−0.43323	−0.000538

Fig. 4 Comparison between the analytical predictions and the numerical integration of the full system: (**a**) transverse displacement and (**b**) harvested power for the high Reynolds number configuration when $R = 10^4 \ \Omega$
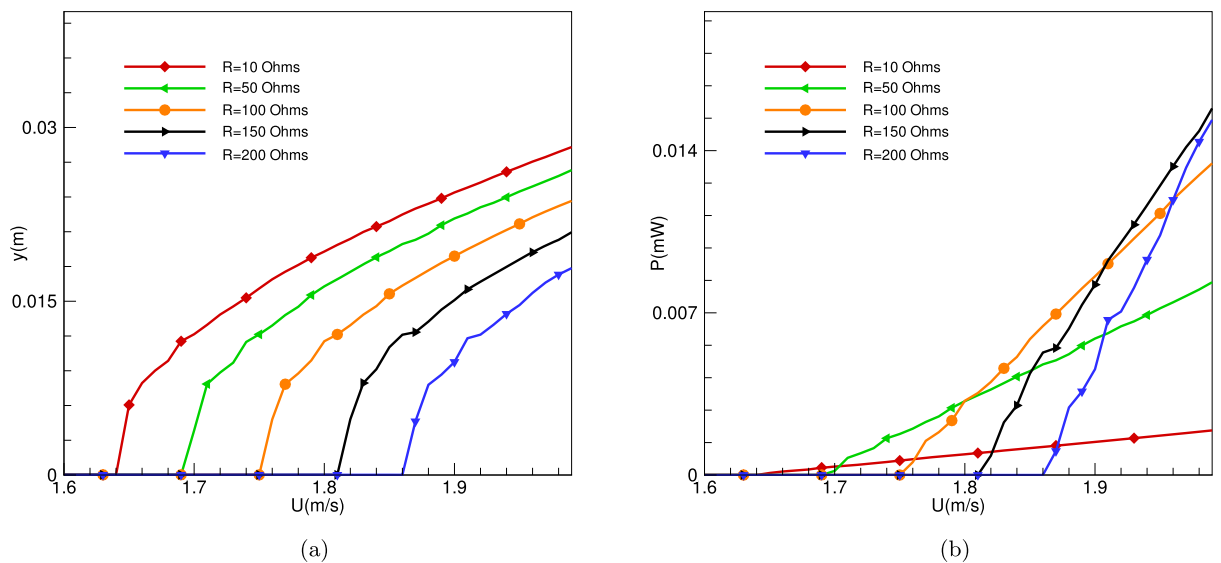

Fig. 5 Variations of the (**a**) transverse displacement and (**b**) harvested power with the freestream velocity for different values of the load resistance in the low Reynolds number configuration

predicts accurately all amplitudes near the onset of galloping. Thus, we conclude that the developed linear and nonlinear analyses provide a methodology to characterize the behavior of transverse galloping near bifurcation for both Reynolds number configurations. In the rest of this investigation, only numerical results are presented.

5 Effects of the load resistance and Reynolds number on the level of harvested power and transverse displacement

The effects of the load resistance on the transverse displacement and harvested power in the low Reynolds number configuration are shown in Figs. 5(a) and 5(b),
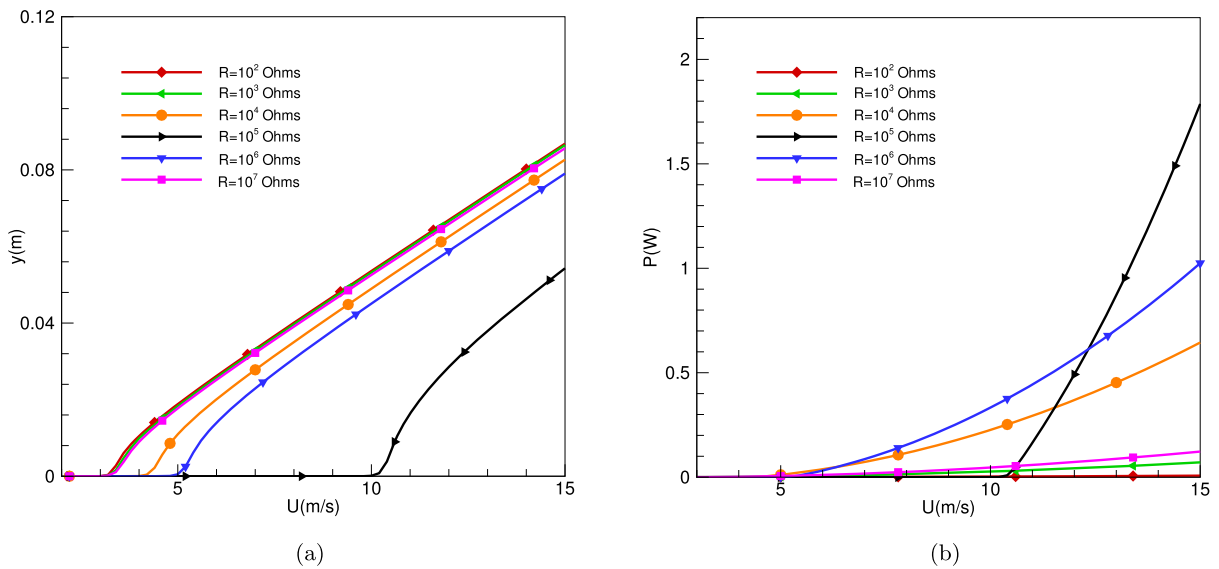
Fig. 6 Variations of the (**a**) transverse displacement and (**b**) harvested power with the freestream velocity for different values of the load resistance in the high Reynolds number configuration

respectively. The plots show that increasing the load resistance results in an increase in the onset speed of galloping. Furthermore, the transverse displacement decreases at higher load resistances. This is due to the increase in the electromechanical damping with increasing load resistance. On the other hand, we note that the harvested power increases with the load resistance. Particularly, the level of harvested power is around 0.015 mW for a freestream velocity near 2 m/s.

In the high Reynolds number configuration (freestream velocity between 2 m/s and 15 m/s), we show in Figs. 6(a) and 6(b) variations of the oscillation amplitudes and harvested power with the freestream velocity over a wide range of electrical load resistance. The results show that varying the load resistance changes the onset speed of galloping. Particularly, this speed is the largest when the load resistance has a value near $R = 10^5$ Ω. The results also show that the load resistance impacts the amplitude of the transverse displacement. Particularly, for $R = 10^5$ Ω, the transverse displacement is the smallest because the electromechanical damping is the highest. Inspecting the curves in Fig. 6(b), we note that an increase in the load resistance is not accompanied with an increase in the harvested power. Rather, there is an optimum value of the load resistance for maximizing the harvested power. This maximum level is associated with the minimum transverse displacement obtained by using a load re-

sistance of about 10^5 Ω. For this load resistance, the power that can be generated is around 1.7 W for a wind speed of about 15 m/s. However, the onset of galloping for this configuration is the highest with the wind speed being near 10 m/s. Furthermore, for a wind speed of 4 m/s, this harvester can generate 0.9 mW and 1.2 mW when $R = 10^3$ Ω and $R = 10^7$ Ω, respectively, and the displacement is $0.75D$.

6 Conclusions

We have investigated the concept of exploiting the galloping phenomenon of a square cylinder to harvest energy over different ranges of wind speeds (Reynolds numbers). The analysis shows that the electrical load resistance and the Reynolds number play an important role in determining the onset of galloping and the harvested power. The harvested energy at high Reynolds numbers is much larger than that at Reynolds numbers below 200. In the low Reynolds number applications, the harvested power can be enhanced by increasing the load resistance. In the high Reynolds number applications, the harvested power can be optimized, with minimum displacement, by properly choosing the load resistance. However, this choice may result in a configuration in which the onset speed of galloping is relatively high.

References

1. Muralt, P.: Ferroelectric thin films for micro-sensors and actuators: a review. J. Micromech. Microeng. **10**, 136–146 (2000)

2. Gurav, S.P., Kasyap, A., Sheplak, M., Cattafesta, L., Haftka, R.T., Goosen, J.F.L., Van Keulen, F.: Uncertainty-based design optimization of a micro piezoelectric composite energy reclamation device. In: 10th AIAA/ISSSMO Multidisciplinary Analysis and Optimization Conference, Albany, NY, pp. 3559–3570 (2004)

3. Inman, D.J., Grisso, B.L.: Towards autonomous sensing. In: Proc. Smart Structures and Materials Conference, San Diego, CA, p. 61740T. SPIE, Bellingham (2006)

4. Roundy, S., Wright, P.K.: A piezoelectric vibration-based generator for wireless electronics. J. Smart Mater. Struct. **16**, 809–823 (2005)

5. Capel, I.D., Dorrell, H.M., Spencer, E.P., Davis, M.W.: The amelioration of the suffering associated with spinal cord injury with subperception transcranial electrical stimulation. Spinal Cord **41**, 109–117 (2003)

6. Sodano, H.A., Inman, D.J., Park, G.: A review of power harvesting from vibration using piezoelectric materials. Shock Vib. Dig. **36**, 197–205 (2004)

7. Anton, S.R., Sodano, H.A.: A review of power harvesting using piezoelectric materials (2003–2006). J. Smart Mater. Struct. **16**, 1–21 (2006)

8. Erturk, A., Inman, D.J.: On mechanical modeling of cantilevered piezoelectric vibration energy harvesters. J. Intell. Mater. Struct. **19**, 1311–1325 (2008)

9. Erturk, A., Inman, D.J.: A distributed parameter electromechanical model for cantilevered piezoelectric energy harvesters. ASME J. Vib. Acoust. **130**, 041002 (2008)

10. Abdelkefi, A., Najar, F., Nayfeh, A.H., Ben Ayed, S.: An energy harvester using piezoelectric cantilever beams undergoing coupled bending-torsion vibrations. J. Smart Mater. Struct. **20**, 115007 (2011)

11. Abdelkefi, A., Nayfeh, A.H., Hajj, M.R.: Global nonlinear distributed-parameter model of parametrically excited piezoelectric energy harvesters. Nonlinear Dyn. **67**, 1147–1160 (2011)

12. Abdelkefi, A., Nayfeh, A.H., Hajj, M.R.: Effects of nonlinear piezoelectric coupling on energy harvesters under direct excitation. Nonlinear Dyn. **67**, 1221–1232 (2011)

13. Bryant, M., Garcia, E.: Energy harvesting: a key to wireless sensor nodes. Proc. SPIE **7493**, 74931W (2009)

14. Erturk, A., Vieira, W.G.R., De Marqui, C., Inman, D.J.: On the energy harvesting potential of piezoaeroelastic systems. Appl. Phys. Lett. **96**, 184103 (2010)

15. De Marqui, C., Erturk, A., Inman, D.J.: Piezoaeroelastic modeling and analysis of a generator wing with continuous and segmented electrodes. J. Intell. Mater. Syst. Struct. **21**, 983–993 (2010)

16. Sousa, V.C., de Anicezio, M., De Marqui, C., Erturk, A.: Enhanced aeroelastic energy harvesting by exploiting combined nonlinearities: theory and experiment. J. Smart Mater. Struct. **20**, 094007 (2011)

17. Abdelkefi, A., Nayfeh, A.H., Hajj, M.R.: Modeling and analysis of piezoaeroelastic energy harvesters. Nonlinear Dyn. **67**, 925–939 (2011)

18. Abdelkefi, A., Nayfeh, A.H., Hajj, M.R.: Design of piezoaeroelastic energy harvesters. Nonlinear Dyn. **68**, 519–530 (2012)

19. Abdelkefi, A., Nayfeh, A.H., Hajj, M.R.: Enhancement of power harvesting from piezoaeroelastic systems. Nonlinear Dyn. **68**, 531–541 (2012)

20. Abdelkefi, A., Hajj, M.R., Nayfeh, A.H.: Sensitivity analysis of piezoaeroelastic energy harvesters. J. Intell. Mater. Syst. Struct. **23**, 1523–1532 (2012)

21. Den Hartog, J.P.: Mechanical Vibrations. McGraw-Hill, New York (1956)

22. Parkinson, G.V., Smith, J.D.: The square prism as an aeroelastic nonlinear oscillator. Q. J. Mech. Appl. Math. **17**, 225–239 (1964)

23. Parkinson, G.V.: Mathematical models of flow-induced-vibrations of bluff bodies. In: Flow-Induced Structural Vibrations, pp. 81–127. Springer, Berlin (1974) (A75-15253 04-39)

24. Parkinson, G.V.: Phenomena and modelling of flow-induced vibrations of bluff bodies. Prog. Aerosp. Sci. **26**, 169–224 (1989)

25. Belvins, R.D.: Flow-Induced Vibration. Krieger, Florida (1990)

26. Naudascher, E., Rockwell, D.: Flow-Induced Vibrations, An Engineering Guide. Dover, New York (1994)

27. Karakevich, M.I., Vasilenko, A.G.: Closed analytical solution for galloping aeroelastic self-oscillations. J. Wind Eng. Ind. Aerodyn. **65**, 353–360 (1996)

28. Laneville, A., Gartshore, I.S., Parkinson, G.V.: An explanation of some effects of turbulence on bluff bodies. In: Proc. of the Fourth International Conference on Wind Effects on Buildings and Structures, pp. 333–341. Cambridge University Press, Cambridge (1977)

29. Alonso, G., Meseguer, J., Prez-Grande, I.: Galloping instabilities of two-dimensional triangular cross-section bodies. Exp. Fluids **38**, 789–795 (2005)

30. Alonso, G., Meseguer, J., Prez-Grande, I.: Galloping stabilities of two-dimensional triangular cross-sectional bodies: a systematic approach. J. Wind Eng. Ind. Aerodyn. **95**, 928–940 (2007)

31. Novak, M., Tanaka, H.: Effect of turbulence on galloping instability. ASCE J. Eng. Mech. Div. **100**, 27–47 (1974)

32. Novak, M.: Aeroelastic galloping of prismatic bodies. ASCE J. Eng. Mech. Div. **96**, 115–142 (1969)

33. Barrero-Gil, A., Sanz-Andres, A., Roura, M.: Transverse galloping at low Reynolds number. J. Fluids Struct. **25**, 1236–1242 (2009)

34. Barrero-Gil, A., Alonso, G., Sanz-Andres, A.: Energy harvesting from transverse galloping. J. Sound Vib. **329**, 2873–2883 (2010)

35. Sohankar, A., Norberg, C., Davidson, L.: Low-Reynolds number flow around a square cylinder at incidence: study of blockage, onset of vortex shedding and outlet boundary conditions. Int. J. Numer. Methods Fluids **26**, 39–56 (1998)

36. Barrero-Gil, A., Sanz-Andres, A., Alonso, G.: Hysteresis in transverse galloping: the role of inflection points. J. Fluids Struct. **25**, 12–15 (2009)

37. Nayfeh, A.H.: Method of Normal Forms. Wiley Interscience, Berlin (2011)